Supplementary information for

Unravelling non-adiabatic pathways in the mutual neutralization of hydronium and hydroxide

Alon Bogot[1], Mathias Poline[2], MingChao Ji[2], Arnaud Dochain[2], Stefan Rosén[2], Henning Zettergren[2], Henning T. Schmidt[2], Richard D. Thomas[2] and Daniel Strasser[1*]

[1]Institute of Chemistry, The Hebrew University of Jerusalem; Jerusalem, 9190401, Israel.

[2]Department of Physics, Stockholm University; Stockholm, SE-10691, Sweden.

Experimental setup

The experimental setup for mutual neutralization (MN) studies was previously described for studies of the undeuterated hydronium and hydroxide system.[12–15] Briefly, Fig S1 shows the schematic layout of the two electrostatic storage rings in DESIREE.[48,49] D_3O^+ ions were formed in a ECR ion source, while OD^- anions were formed in a SNICS sputter ion source.[50] The D_3O^+ and OD^- ion beams were injected to the rings at velocities corresponding to kinetic energies of 36 keV and 26 keV, respectively. The common section of the two rings allows to study MN reactions in a merged-beams configuration. Low energy collisions were confined to a 76 mm long drift tube that allows a fine control of the collision energy by applying a potential, U_0, which accelerates the anions and decelerates the cations. Here, in order to match both ion beams velocities to ~ 5.5×10^5 m/s and achieve cold collisions, a U_0 = 1915 V potential was applied. Neutral products produced from these collisions escape the storage rings and hit a 75 mm diameter microchannel-plate (MCP) detector, which is equipped with a phosphor screen anode, and located 1521 mm downstream. The 3D time and position data presented in this work was recorded by a time and position sensitive TPX3CAM camera,[51,52] in which individual pixels independently record the time of arrival and time over threshold of the measured optical signals of coincident neutral hits on the detector.

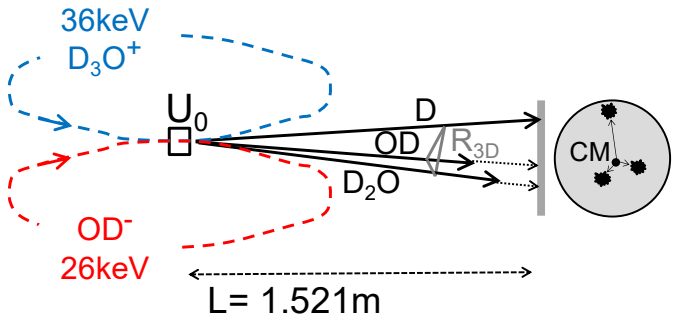

Fig. S1. Schematic representation of the experimental setup. *The DESIREE facility has two storage rings which contain a merged section composed of several drift tubes. One ring storing a 36 keV D_3O^+ cation beam and the other ring a 26 keV OD^- anion beam. The black arrows show a schematic three-body D_2O + OD + D breakup event.*

Two-body analysis & Proton transfer isotope effect

As in Bogot et al,[13] the spectrum of coincident pairs was found to be dominated by partially detected 3-body breakup events. This, primarily due to the ~30% detection efficiency of the MCP detector in the cryogenic DESIREE environment.[13,53] The blue bars in Fig S2a show the measured 3D distance spectrum for coincident pairs with equal and opposite recoil, that could be potentially attributed to the $2D_2O$ product channel, according to total CM momentum conservation. The gray region in Fig. S2a shows the background contribution, which was estimated based on events in which the total CM momentum of the neutral fragments did not match the total momentum of the parent ions (assuming $2D_2O$ products). The red region shows the evaluated contribution of the above mentioned partially detected 2OD + D_2 and D_2O + OD + D three-body breakup events to the two-body spectrum. Similar to Bogot et al,[13] this contribution was derived based on the measured three-body events. Figure S2b shows the same analysis for the undeuterated experiment reported in Bogot et al,[13] where the cyan region indicates an over ~2% contribution from $2H_2O$ events. In comparison, the number of excess events for the deuterated system, beyond the contribution of partially detected channels, was estimated to be below an <1% limit for the $2D_2O$ channel. This indicates the effective suppression of the proton-transfer mechanism in the fully deuterated system. One can also note due to variation in experimental conditions, the undeuterated data had lower levels of random coincidence background. Furthermore, we tentatively attribute the difference in the shape of partially detected background peaks to a higher effect of an undetected D versus H recoil on the R_{3D} separation of the measured two heavy fragments.

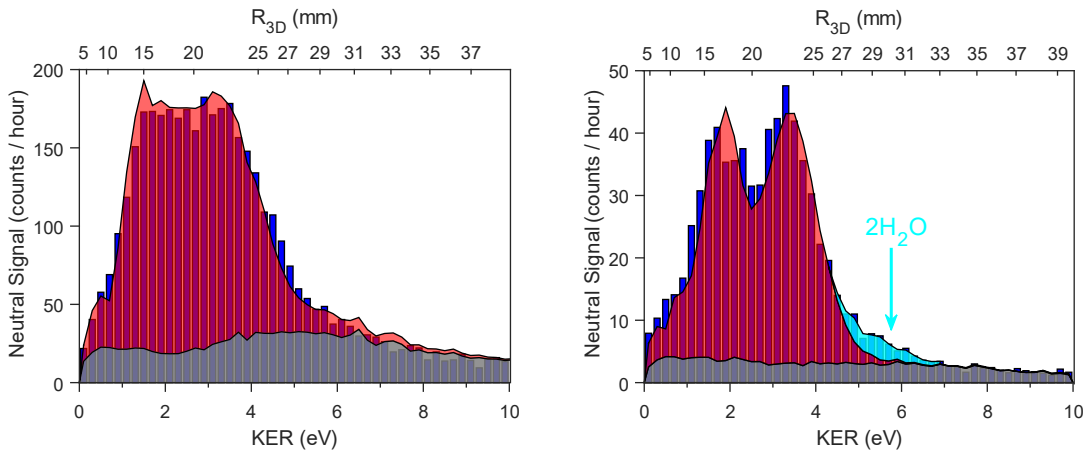

Fig S2: Coincident two-body product channel analysis. *In both panels (a) and (b), the blue bars show the total KER spectrum, where the KER was derived from the measured 3D distance between the fragments as they hit the detector, assuming a $2D_2O$ or $2H_2O$ breakup respectively. In both panels the gray region indicates the background contribution (evaluated from events not conserving CM momentum). The red region indicates the contribution of three-body breakup events to the two-body spectrum (evaluated from the measured three-body events). The remaining events which are not contained by either the gray or red regions are attributed to contribution of real MN two-body events. The cyan region in panel (b) indicates an over ~2% contribution from real $2H_2O$ events.*

Channel assignment by PCA analysis

As mentioned in the main text, under the current experimental conditions, momentum conservation is insufficient to distinguish between the two possible 3-body product channels. Therefore, additional aspects must be considered. In Bogot et al,[11] we described how the measured KER can be used to distinguish between different product channels. Here, we implemented a more general approach based on principal component analysis (PCA) to distinguish between the 3-body channels. The PCA was performed on a total of 6 parameters, including the center of mass displacement, total KER, and the energy fraction of the light mass fragment. All three, calculated assuming each of the two possible channels. Figure S3a shows the measured distribution as a function of the two leading PCA components that are largely dependent on the total KER in each event and the kinetic energy fraction of the light fragments (same as Fig 3a in the main text). In contrast with the assignments described in Fig 3 of the main text, panels (b) and (c) show the KER spectra when assuming an opposite assignment: i.e., that the left-hand-side corresponds to D_2O + OD + D channel and the right-hand-side to 2OD + D_2. Clearly, this alternative assignment is not possible as the KER distribution of the 2OD +D2 channel shown in Fig S3c exceeds the total available energy for this channel, indicated by the dashed vertical line.

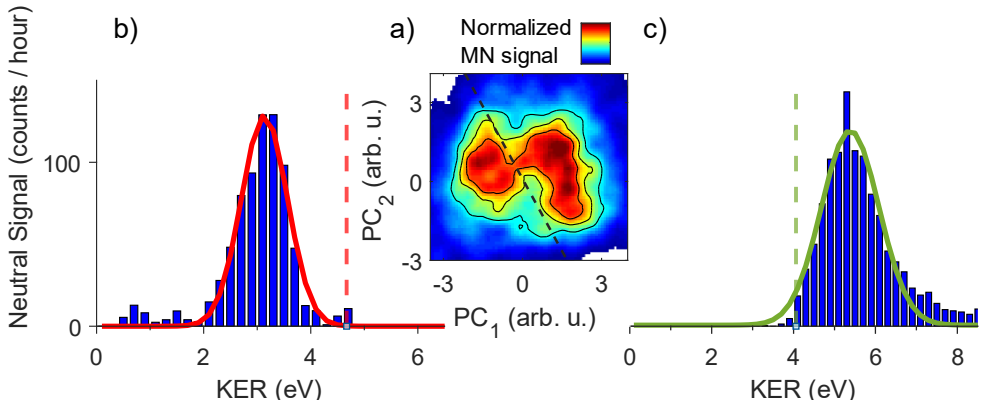

Fig S3: Opposite three-body product channel assignment and KER analysis. *Panel (a) presents the distribution of the coincident 3-body events as a function of the most significant components of the PCA analysis. Events on both sides of the dashed black line were attributed to different 3-body product channels. Events of the left-hand side feature were attributed to the D_2O + OD + D channel, which KER distribution is shown in panel (b). While events on the right-hand side were attributed to the 2OD+D_2 channel, which KER distribution is shown in panel (c). Dashed vertical lines in panels (b) and (c) indicate the maximal available energy in the respective product channel.*

Systematic test of the PCA analysis for the undeuterated $H_3O^+ + OH^-$ system

For completeness, Fig S4 shows the result of PCA assisted analysis of the undeuterated data that is found to be in agreement with the earlier reported analysis.[13] The yield distribution as a function of the two dominant PCA components is shown in panel (a), while panels (b) and (c) present the KER distributions for the 2OH + H_2 and H_2O + OH + H product channels respectively, while attributing the left feature in the PCA distribution to the 2OH + H_2 and the right side feature to H_2O + OH + H. The analysis confirms the earlier reported 3:1 branching ratio between the channels and that the excess energy in each channel (indicated by the vertical dashed lines) contributes mainly to the KER and not to the internal excitation of the molecular products.

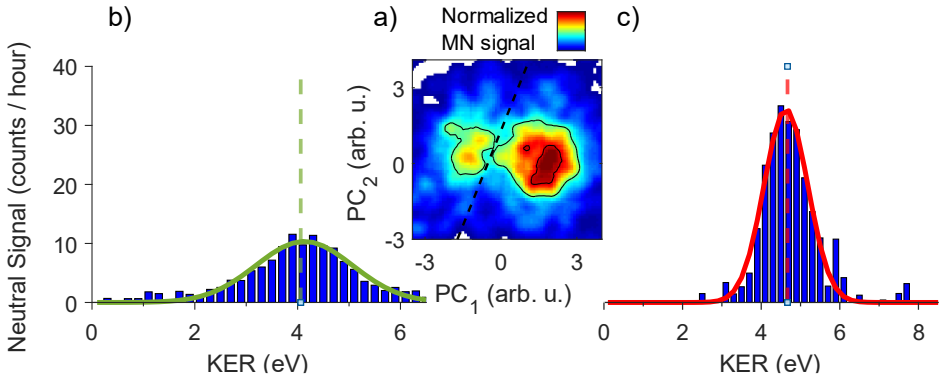

Fig S4: Undeuterated three-body product channel assignment and KER analysis. *Panel (a) presents the distribution of the coincident 3-body events as a function of the most significant components of the PCA analysis. Events on both sides of the dashed black line were attributed to different 3-body product channels. Events of the left-hand side feature were attributed to the 2OH + H_2 channel, which KER distribution is shown in panel (b). While events on the right-hand side were attributed to the H_2O + OH + H channel, which KER distribution is shown in panel (c). Dashed vertical lines in panels (b) and (c) indicate the maximal available energy in the respective product channel.*

Kinetic energy of the OD products

Once a sequential dissociation mechanism is determined, the kinetic energy of the initial OD product can be related to the initial KER by dividing it by the ratio of the D_3O mass and the total mass (22/40). Figures S5 and S6 present the kinetic energy distribution of the OD products. The measured distributions are fitted with Gaussian functions peaking at ~1.9 and ~0.8 eV for the D_2O + OD + D and 2OD + D_2 respectively. Although this analysis may be affected by the limited ability of distinguishing OD from D_2O, or the 1st and 2nd OD. Nevertheless, as discussed in the main text, the peak kinetic energy of the OD product is in agreement with the simulated sequential dissociation mechanisms that are best fitting to the measured Dalitz plot distributions of the two channels.

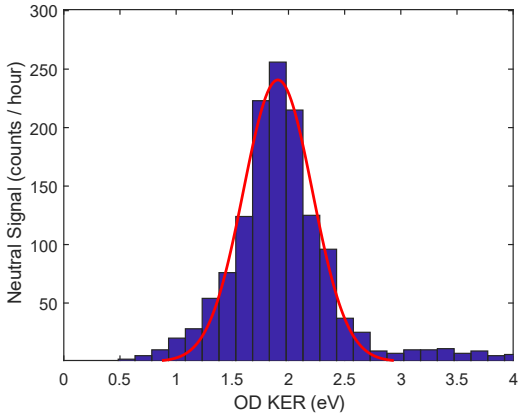

Fig S5: Kinetic energy of the OD fragment for the D_2O + OD + D channel. *Kinetic energy distribution of measured kinetic energy of the neutral OD fragment in the center of mass frame, arriving from the initial electron transfer process for the D_2O + OD + D product channel. The red curve shows a fitted gaussian function centered at 1.9 eV.*

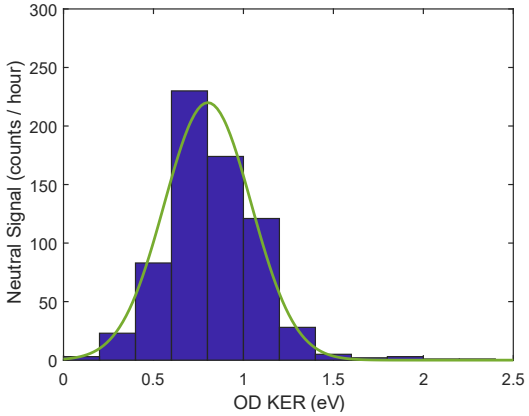

Fig S6: Kinetic energy of the OD fragment for the 2OD + D_2 channel. *Kinetic energy distribution of measured kinetic energy of the neutral OD fragment in the center of mass frame, arriving from the initial electron transfer process for the 2OD + D_2 product channel. The green curve shows a fitted gaussian function centered at 0.8 eV.*

Estimates of the IP and electronic excitation energy of [D_3O]

As described in the main text, Monte Carlo simulations were carried out in order to determine best fitting initial KER between the OD and intermediate D_3O products of electron-transfer. Figure S7 demonstrates the optimization process in which the simulated initial KER was varied, and the final Dalitz plot for the D_2O + OD + D channel was compared with experimental data. Specifically, we compare the distinct peak of the simulated KER fraction of the D product, ε_D, with the measured ε_D peaking at ~20%, indicated by the horizontal dashed line. Figure S7 insets show three of the simulated Dalitz plots: for the best fitted simulation with an initial KER of 3.6 ± 0.1 eV. For an initial KER that is too low and an initial KER that is clearly too high. Error bars were estimated based on the finite size of the ε_D bins, reflecting the experimental statistics.

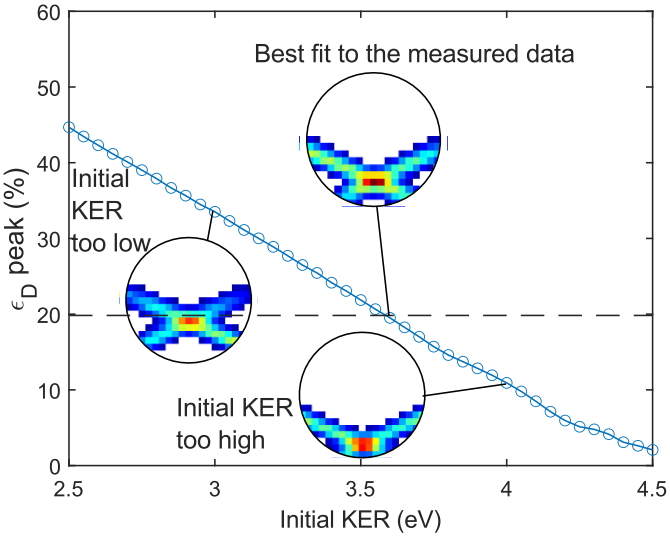

Fig S7: Simulated three-body correlation distributions as a function of the initial KER following electron-transfer. *The peak position of the mass scaled kinetic energy fraction ε_D (the vertical axis of the Dalitz plot), simulated for the D_2O + OD + D as a function of the initial KER. The horizontal dashed line indicates the experimentally measured ε_D peak position. Dashed horizontal line indicates the experimental ε_D peak. The insets show three examples of the calculated Dalitz plots for different initial KER values.*

The [H_3O] IP can then be estimated as the measured ~3.6 eV initial KER following electron transfer plus the well-established ~1.8 eV electron affinity of hydroxide,[26] Table 1 provides a summary of reported theoretical and experimental estimates of the [H_3O] IP. The current data is therefore in agreement with the theoretical calculation of Luo et al.[27] As described in the main text, the same analysis for the 2OD + D_2 channel shows a 2 ± 0.1 eV lower IP, in agreement with the excitation energy of the [H_3O] first excited state predicted by Luo et al.[27]

Table 1: [H_3O] energetics.

	Gellene & Porter.[45]	Luo et al.[27]	Simons et al.[28]	Present study
IP [H_3O] (eV)	4.3	5.4	5.3	5.4 ± 0.1
E [H_3O^*] (eV)	1.7	2.1	-	2.0 ± 0.1